Angular efficiency dependance of semileptonic W pair decays at the ILC

Matthew Koster

University of Cambridge

FLC group, Summer Student Programme

September 4, 2019

Supervisor: Jakob Beyer

Abstract

An analysis is performed on the muon semi-leptonic decay channel of a pair of W bosons produced in $500\,\mathrm{GeV}$ center of mass energy $e_L^- e_R^+$ collisions at the ILC. The invisible decay products are reconstructed using conservation laws and the visible reconstructed data. Angular distributions defining the semileptonic decay are extracted from generator level particles and cuts are applied on the reconstructed particles to obtain the angular dependance of the reconstruction efficiency. The analysis reveals an angular dependence of the efficiency which is not currently modelled in the Electroweak polarisation fit for the ILC.
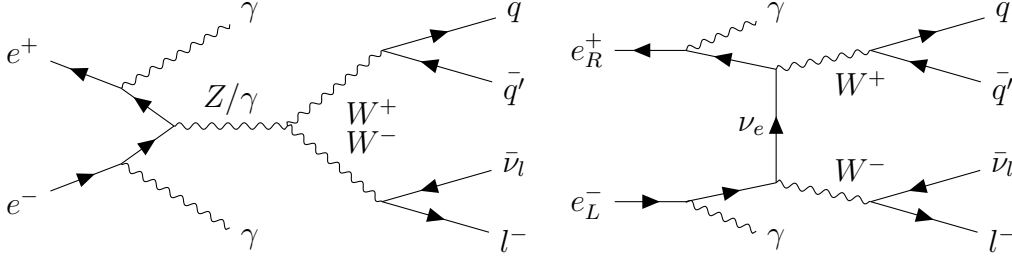
Contents

Figure 1: Lowest order Feynman diagram of semileptonic W pair decay in the $\mu\bar{\nu}q\bar{q}'$ final state at e^+e^- colliders, with two ISR photons emitted. A s-channel (left) and t-channel (right) diagram are shown. Alternately the W^+ could decay leptonically and the W^- hadronically, which would result in a $\mu^+\nu q\bar{q}'$ final state (not drawn).

1 Introduction

Analysis of the pair production of W bosons in an electron positron collider (see Figure. 1) is an important tool for probing the chiral nature of the electroweak interaction for physics Beyond the Standard Model (BSM). A particles chirality is determined by whether the particle transforms in a right- or left-handed representation of the Poincaré group. For massless particles, which travel at the speed of light in all frames, this is equivalent to its helicity which is defined by the projection of the particles spin vector onto its momentum vector. If this projection is positive the helicity is right-handed, and if it is negative the particle is left-handed. Chirality is a bit more subtle for massive particles, because the direction of their momentum is not frame invariant. The charged W bosons only couple to left handed particles and right handed anti-particles, and so the t-channel W pair production mode is only active if the initial state consists of a left-handed electron and right-handed positron ($e_L^- e_R^+$). The s-channel, however, is active as long as the electron and position have opposite chirality. This means by adjusting the ratio of e_L^- and e_R^+ in the particle beams of a collider, it is possible to switch the t-channel W pair production on and off. This can be used to probe the chiral structure of the electroweak interaction. Furthermore, the triple gauge vertex in the s-channel is a direct consequence of the chiral nature of the electroweak interaction and understanding this W pair production will help us better probe this vertex in a hunt for BSM effects.

The data analysed in this report contains events where an initial state $e_L^- e_R^+$, with a center of mass energy of 500 GeV, produces a pair of W bosons, which in turn decay semileptonically. A semileptonic decay is defined such that one of the W bosons decays leptonically into a lepton and a neutrino, and the other boson decays hadronically into a pair of quarks. In this report, the muon signal of this decay is analysed. From the reconstruction of this interaction, the angular dependence of the detector and reconstruction efficiency is be analysed. This efficiency can then be implemented into the Electroweak Polarisation fit for the International Linear Collider (ILC), which currently assumes a global efficiency value of 60%, and its effects analysed further.

In Section. 2 the analysis methods used to extract the 4-momenta information of the final state particles will be discussed, along with a description of the angular distributions that are used. A discussion of how the efficiency of the reconstruction and its angular dependence are evaluated, and how they perform, is conducted in Section. 3. Finally, the findings of this report are concluded in Section. 4.

2 Final state 4-momenta analysis

This analysis reconstructs the 4-momenta of the particles in the hard collision, using data from 500 GeV ILC simulations containing generator level particles and reconstructed particles. Then several variables used in the analysis in Section. 3 are evaluated and stored in a .root file. In order to do this it must use some kinematically derived formulae (Section. 2.3.1) to reconstruct the invisible 4-momenta contribution of the neutrino and any initial state radiation (ISR)[1]. This section contains the details of each part of this analysis.

2.1 Beam Background Removal

In a particle collider, to increase the probability of a hard collision, a 'bunch' [1] of particles are collided and due to the low cross-section one may expect only one hard interaction to occur. These other particles, however, do interact with each other which may produce particles that leave traces in the detector and so will generate so-called beam background. This is modelled in the collision simulation so these particles get reconstructed. These reconstructed particles from the background must be removed before analysis of the hard collision can be conducted.

The FastJetProcessor [2] is used to conduct such beam background removal from the reconstructed particle collection. Another method of background removal is by using generator level information to help remove the background from the reconstructed particles, this is done with the TrueJet processor [3]. This is a liberty that is only possible because the collisions are simulated, therefore it is not possible at an active detector and is referred to in this report as 'cheating overlay removal'. The later method is used to explore the sensitivity of the reconstruction to this beam background removal in Section. 2.3.4.

2.2 4-momenta Reconstruction

For the generator level particles, each of the particles in the hard collision are directly extracted from the collection using their element number. It is then a simple task of inputting their energies and momenta into a TLorentzVector [4]. The W bosons 4-momenta are then calculated by addition of the 4-momenta of its decay products.

The IsolatedLeptonTaggingProcessor [5] is used to extract the hard collision lepton[2] from the reconstructed particles. The FastJetProcessor [2] extracts the two reconstructed quarks. The 4-momenta of these final state particles and subsequently that of the hadronically decaying W boson (W_{had}) can then be reconstructed[3].

Reconstruction of the leptonically decaying W boson (W_{lep}) requires a bit more thought, this is because of the neutrino and the ISR photons, which leave no signal in the detector. This challenge is discussed in detail in the following section.

---

[1]Photons radiated by e^- or e^+ before collision

[2]If it correctly reconstructs the lepton, sometimes it returned zero particles, sometimes more than one, this is cut on later

[3]It should be noted that running the LcfiplusProcessor [6] did improve this reconstruction

2.3   Neutrino and ISR Corrections

2.3.1   The invisible system

The leptonically decaying W boson is reconstructed by summing the 4-momenta of the extracted lepton and the neutrino, however, the neutrino does not leave a signal in the detector. In addition, there is some initial state radiation of photons (ISR) which are aligned enough to the beam pipe to not be detected. This results in an 'invisible' system that is not at all detected by the detector, and, to obtain complete information about the W bosons, this invisible system has to be reconstructed.

The chosen method for reconstruction of the invisible system arises purely from conservation laws[4]. The reconstructed visible system is considered as being the hadronically decaying W boson plus the isolated lepton ($p^\mu = (E, p_x, p_y, p_z)$), and the invisible system as the accompanying neutrino and an ISR photon, travelling parallel to the beam. The total center of mass energy is assumed to be 500 GeV and the hard interaction is assumed to take place in the center of mass frame. Conservation of momentum and energy then exactly defines the 4-momenta of the ISR photon and the neutrino. In the simulation there are two ISR photons emitted. This means that when combining the two photons into one 'photon', this 'photon' may have a non zero invariant mass. Furthermore, the ISR photon could be going in either direction with respect to the beam axis, resulting in two solutions.

$$E_\gamma = \frac{\lambda(500 - E) \pm p_z\sqrt{\lambda^2 - [(500 - E)^2 - p_z^2]m_\gamma^2}}{(500 - E)^2 - p_z^2} \tag{1}$$

where $\lambda = \frac{1}{2}[(500 - E)^2 - p^2 + m_\gamma^2 - m_\nu^2]$ has been defined for convenience and no absolute values have been assumed.

The solution that reconstructs the invariant mass of the W boson closer to the currently accepted value of 80.3 GeV [7] is selected. This may shift more of the background into the peak introducing a bias and so the appropriate cut is made to mitigate this [8].

The rest of the unknown variables of momentum and energy are exactly defined from this and can be easily evaluated. As a result the 4-momenta of all of the particles in the hard interaction are known, as required for the analysis.

A simplified form of this equation with $m_\gamma = m_\nu = 0$ is used in Ivan's thesis. Equation. (1) correctly simplifies to this solution as shown in the appendix.

$$E_\gamma = \frac{(500 - E)^2 - p^2}{1000 - 2E \mp 2p_z} \tag{2}$$

It is worth noting at this point that it is numerically possible for the particle reconstruction to result in a visible 4-momenta with a negative λ. It can be seen in the $m_\gamma = m_\nu = 0$ solution that this corresponds to the invisible part of the system having an imaginary invariant mass.

$$\lambda_{m_\gamma, m_\nu = 0} \propto (500 - E)^2 - p^2 = E_{inv}^2 - p_{inv}^2 = m_{inv}^2 \tag{3}$$

---

[4] a full mathematical derivation is included in the appendix for completeness (Appendix. 7.1)
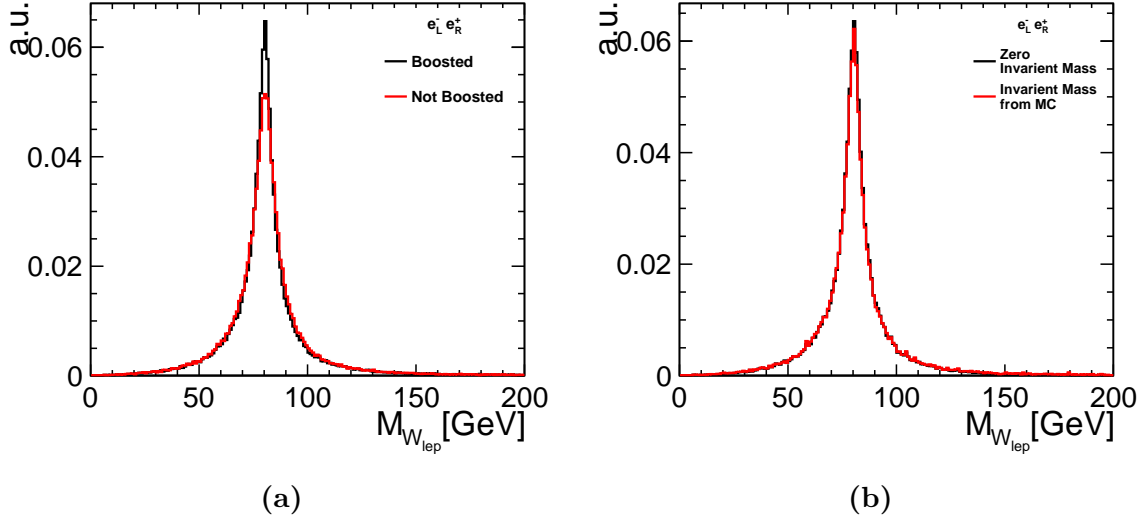
Figure 2: The effect on the reconstructed invariant mass of the leptonically decaying W with different reconstruction methods. (b) A Lorentz boost into the center of mass frame is considered. (b) A non-zero invariant ISR photon mass, obtained from generator level information, is considered.

This is obviously not physical and will affect the solutions attained above. For example as $p_\gamma = \pm E_\gamma$, a negative energy will reverse the direction of the photon. This needs to be handled carefully in the code to avoid inconsistent solutions.

It can be analytically shown that Equation. 1 leads to Equation. 2 when simplified, there is however one subtlety when this is done computationally. The $\sqrt{\lambda^2}$ will computationally evaluate as $|\lambda|$, so if λ is negative it will in effect reverse the effect of the $\pm$ in Equation. 1 and lead to the opposite solution of the simplified form. So it is clear that these negative λ's may cause some issues if the contribution from the m_γ in non-negligible. This is not explored further, because in Section. 2.3.3 it is shown that including the non-zero m_γ contribution from the Monte Carlo has little effect on the solutions attained and so Equation. 2 is used with the $\pm$ swapped accordingly.

From this, the 4-momentum of the leptonically decaying W boson is reconstructed. As a test of performance, the accuracy of the reconstructed invariant mass of this boson is evaluated. By exploring different several variations of this reconstruction the sensitivity of the ISR energy solution is tested in the following analysis.

2.3.2 Center of Mass frame

The e^+e^- collision is incident at a non zero angle. Consequently the total system in detector frame has a non-zero 3-momentum $p^\mu = \left(500 \sin\left(\frac{0.014}{2}\right), 0, 0\right)$ GeV. In theory addition of a boost into the centre of mass frame should result in an improvement in the reconstruction, because the assumption that the total energy is equal to the center of mass energy is only satisfied in this frame. In fact we see that is makes a considerable improvement to the mass peak (Figure. 2a) and is kept in the following analysis.
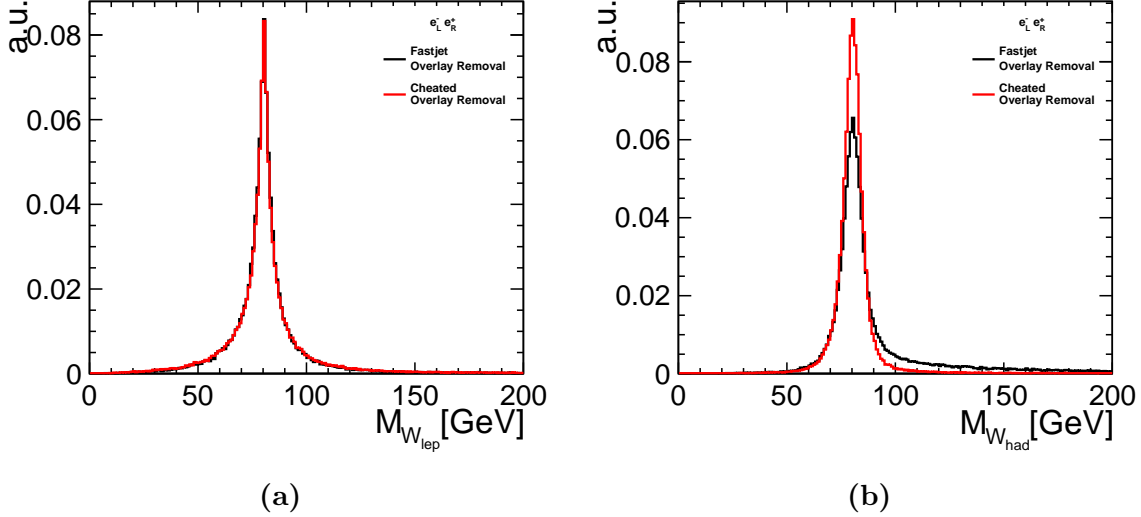
Figure 3: Plots displaying the effect of cheating the beam background removal on the reconstructed invariant mass of the two W bosons, (a) the leptonically decaying W and (b) decaying hadronically.

2.3.3 ISR invarient mass

Another assumption that is tested is the non-zero invariant mass of the ISR photon. As two ISR photons are emitted, but only one photon is modelled in the reconstruction, this modelled photon need not satisfy this constraint. The true invariant mass is obtained from the generator level particles and inputed into Equation. 1, which is derive with this constraint relaxed. Again this is a 'cheat' as this information would not be available in a real detector. This addition had a negligible effect on the reconstructed W mass (see Figure. 2b), which could be due to the size of the photon mass indeed being negligible, even if non-zero.

2.3.4 Beam Background Removal

The third check that is performed is the sensitivity of the reconstructed $m_{W_{lep}}$ to the beam background. This is done by comparing the two different background removal methods suggested in Section. 2.1. It is found that cheating the beam background removal improved the reconstruction of the two quarks, which can be seen in the reconstruction of the invariant mass of the hadronically decaying W boson (Figure. 3). In particular this cheating greatly suppresses an overestimation tail observed in the properly reconstructed particles. This in turn improves the reconstruction of the visible portion of the system. The $m_{W_{lep}}$ on the other hand is generally insensitive to this change. Explaining this is non-trivial due to the fairly complicated nature of the E_γ formula.

2.3.5 Negligible ISR case

The ISR energy formula regularly reconstructs a wide range of energies (of order ± 20 GeV) when the true ISR energy is less than 0.5 GeV(see Figure. 4a). Addition of a third solution to the photon energy formula is implemented, where the photon energy, and hence momentum, is set exactly equal to zero. The conservation laws then directly defined the 4-momenta of the neutrino, as it is then the only contribution to the invisible part of the system. As before the estimate of $m_{W_{lep}}$ is calculated using all three solutions to E_γ and the solution that more accurately reconstructed this mass os chosen. Once again this selection may draw more of the background into the peak and introduce a bias. The extent of this is not explored in this report,
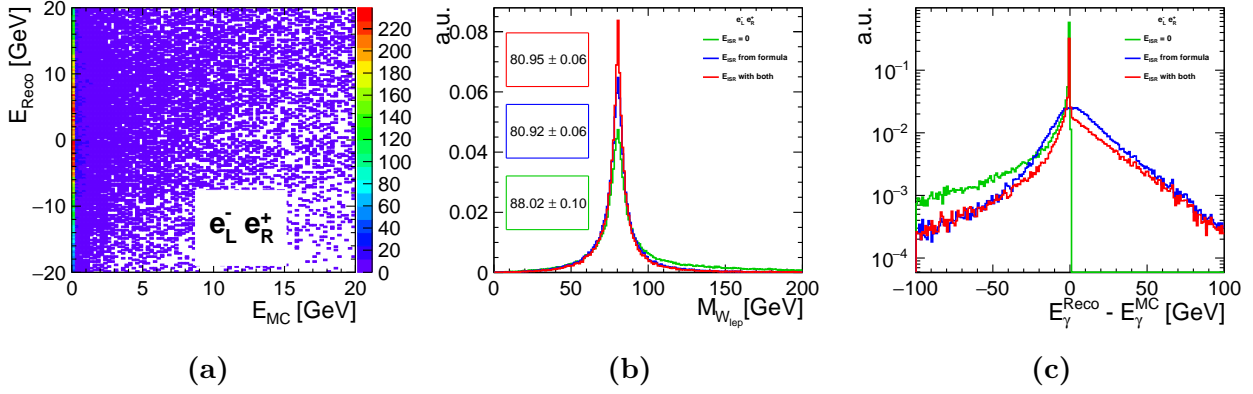
(a)   **(b)**   **(c)**

Figure 4: (a) Reconstructed ISR photon energy against the generator level ISR energy. (b) Reconstruction of the leptonically decaying W mass for the three different E_γ claculation methods . (c) Log histogram showing the reconstruction of E_γ from the three claculation methods.

but it is important to keep into consideration in the following, and any further, analysis. This seems to improve the estimation of $m_{W_{lep}}$ as seen in (Figure. 4b), although it is unclear if this is a true improvement in the method due this bias.

As another check of the performance of this edit, a histogram of just $E_\gamma^{Reco} - E_\gamma^{MC}$ is created (Figure. 4c), to see if this improvement in $m_{W_{lep}}$ is accompanied by an improvement in the estimation of E_γ. Here it can be seen that the addition of the $E_\gamma = 0$ solution reduces the number of under and over estimates quite significantly. The highest peak at zero , however, claimed by the solution where there is no ISR considered at all (green). This means that sometimes an over/under-estimation of the photon energy returns a better reconstruction of the $m_{W_{lep}}$.

2.4   Angle extractions

From this analysis, complete information about the final state particles, and hence the intermediate W pair, is obtained. From this we can evaluate the angular distributions required for the next section of the analysis. This distributions are extracted from generator level particles, as this is what is being used as input to the Electroweak Polarisation fit.

The semileptonic decay of a pair of W bosons is fully described by just 6 angles; the polar coordinates of the $W-$ in the center of mass frame; the polar coordinated of the lepton in the center of mass frame of the W it decayed from; and the polar coordinated of one of the quarks in the center of mass frame of the boson it decayed from. The ϕ coordinate of the $W-$ is expected to be uniformly distributed and so returns no information about the chiral structure and is not considered in the fit. Further, it is hard to assign a charge to the quarks in their reconstruction, so it is not possible to consistently chose one the the quarks to measure its angles. Hence the quarks polar coordinates are also not considered in this analysis. This leaves just 3 angles as defined in Figure. 5, namely the theta coordinate of the W^- in the centre of mass frame (θ_{W^-}), and the theta and phi coordinates of the lepton in the rest frame of the W_{lep} it decayed from (θ_l^* and ϕ_l^*). The polar coordinate system is the same in both frames, with the z axis aligned to the beam-pipe. The same Lorentz boost framework used in Section. 2.3.2 is implemented here and so this is a computationally very simple task, and the extracted angles are put in the root tree.

Table 1: Selection efficiency of sequentially applied cuts. Where the post ISR correction m_W^{lep} is calculated using all 3 possible E_γ solutions. (*) Indicates cuts where the current and Ivan's cuts differ, as discussed in the text.

Order	Cut description	Efficiency [%]			
		My Results			Ivan's Results
		n = 2129	n = 99419		n = 107233
			no cheat	cheat	
0	muon signal	100.00	100.00	100.00	100.00
1	track multiplicity[5] $n_{tracks} \geq 10$	97.13	97.01	96.23	99.996
2	center of mass energy $\sqrt{s} > 100$ GeV	92.29	91.69	84.35	97.96
3	total transverse momentum $P_T > 5$ GeV	91.16	90.47	83.28	96.69
4	total energy $E_{SUM} < 500$ GeV	89.66	89.28	82.70	95.36
5	$\ln(y_+) \in [-12, -3]$ (*)	88.69	88.08	82.47	95.01
6	1 lepton found (*)	80.65	80.77	81.50	78.75
7	pre ISR correction $m_W^{lep} \in [20, 250]$ GeV	78.23	77.94	77.84	76.61
8	tau discrimination[6]	76.05	75.60	75.73	74.07
9	charged lepton (*)	76.05	75.60	75.73	73.51
10	isolation variable[7] $\Delta\Omega_{iso} > 0.5$	76.01	75.58	75.72	73.42
11	post ISR correction $m_W^{lep} \in [40, 120]$ GeV	72.90	72.77	72.33	70.13
12	post ISR correction $m_W^{had} \in [40, 120]$ GeV	63.21	62.92	70.52	66.93
13	$\cos\theta_W > -0.95$	63.02	62.65	70.21	66.78

The resulting angular distributions that are obtained are visible in Figure. 6, where the θ angles have been displayed in terms of their cosine for comparison with previous results [9].

3 Angular dependance of efficiency

The following analysis is performed on data generated using the reconstruction techniques described above, choosing the best of all three E_γ solutions, with $m_\gamma = m_\nu = 0$. Unless otherwise explicitly stated, the beam background removal is not cheated but the Lorentz boost into the centre of mass frame is performed. The analysis is conducted considering only the muon signal of the data set, as this is the focus of this analysis.

3.1 Cut Flow

The efficiency of the reconstruction is evaluated by the percentage of events that are left after a series of cuts (see Table. 1) have been applied. These cuts are applied for various reasons, but generally are used to ensure the reconstruction is performing properly and to remove unwanted backgrounds. The cuts are performed on reconstructed data to assess how the detector and reconstruction techniques are performing. The results of this analysis are then compared to previous studies by Ivan Marchesini [8]. Further, the efficiencies are evaluated again by cheating the beam background removal, and by applying the additional initial cut that the ISR energy is small ($E_\gamma^{MC} < 1$ GeV). The final plot is made to see if the ISR made a considerable contribution to the efficiency of the cuts. The resulting cut flow diagram (Figure. 7) displays all of this information in one cut flow diagram, showing the resulting efficiency after each sequential cut
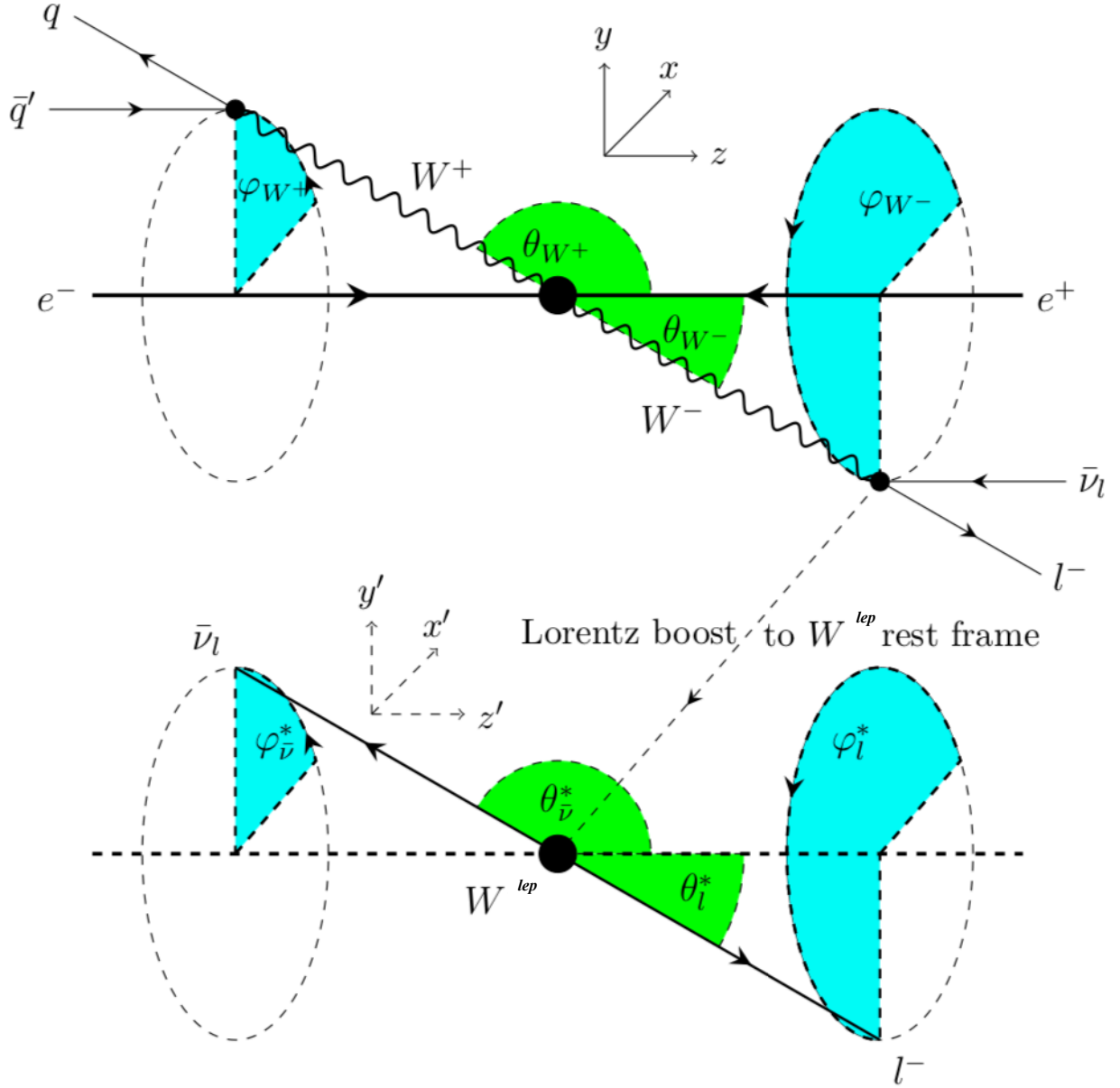
Figure 5: Angle definition for the 4-fermion final state from W^- pair production in the semileptonic channel in which the W decays leptonically. In the top part, the production angles θ_{W^-} and θ_{W^+} are defined by the axis of the initial colliding particles and the direction for the respective boson. The azimuthal angles ϕ_{W^-} and ϕ_{W^+} describe the rotation around the axis of the initial colliding particles.

The bottom picture shows the angular definition of the decay products of the W^{lep} boson in its rest frame. It shows the polar angles θ_l^* and $\theta_{\bar{\nu}}^*$ and the azimuth angles ϕ_l^* and $\phi_{\bar{\nu}}^*$ of the corresponding leptons. The denotes quantities in the rest frame of the W^{lep} boson. (Edited from [9])
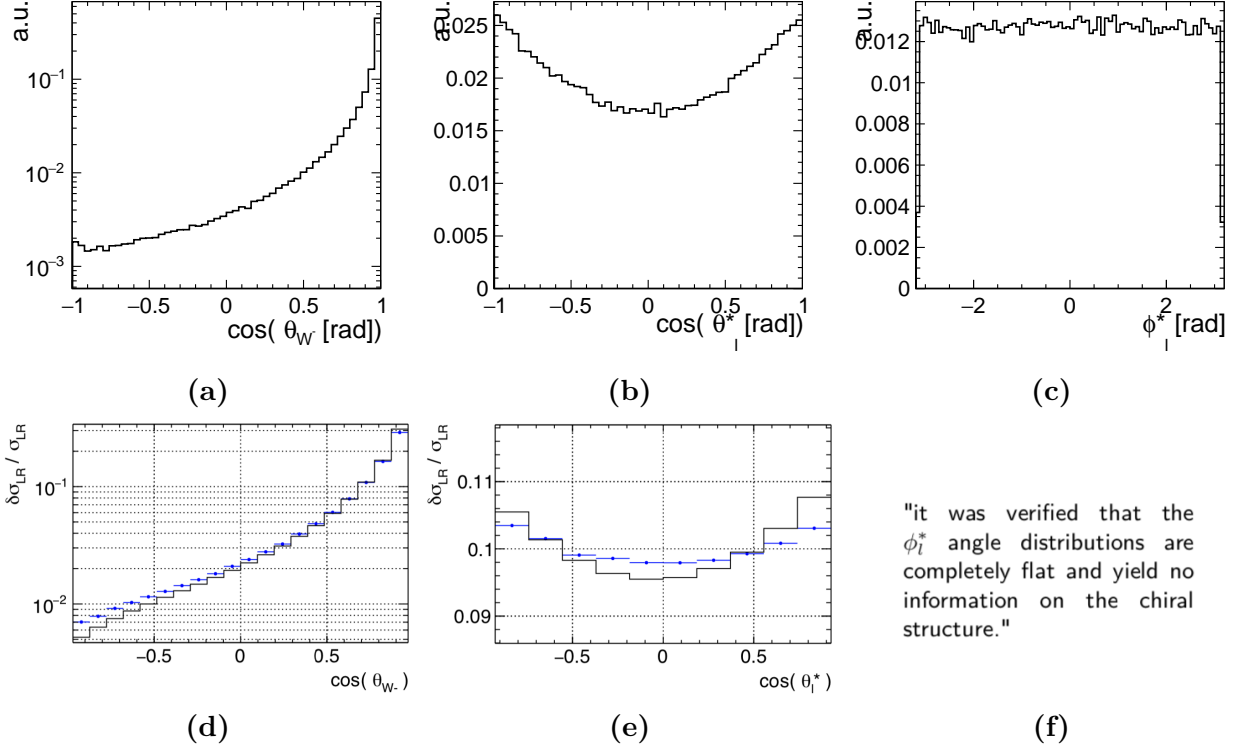
Figure 6: (a), (b) and (c) are the extracted angles as defined in Figure. 5.
(d), (e) are the associated angular distributions currently being input into the Electroweak
Polarisation Fit [9] and (f) is an extract from the text describing the ϕ_l^* distribution

There are a few subtle differences between the cuts that Ivan and the cuts made in this analysis, due to the reconstruction methods each implemented. The first is the cut on the jet reconstruction variables y_+ and y_-. In this analysis FastJets [2] is forced to reconstruct two jets, corresponding to the 2 quarks, and physically this is the minimum number of jets that can occur, as single quark cannot be created. This means the cut on the y_- variable that Ivan makes is unphysical in this analysis. Ivan applies this cut because he also considered final states with 4 quarks. The lepton cut that is made here make is also different to Ivans. The IsolatedLeptonTaggingProcessor is used, so the implemented cut is that a single isolated lepton is reconstructed. There are a considerable number of events where the processor reconstructed zero particles, and so this cut can be significant. Ivan on the other hand used a jet reconstruction processor with a specific energy cut to reconstruct isolated leptons. The final difference is that Ivan makes a 'charged lepton' cut, a similar cut is not made in this analysis and so the corresponding efficiency will not change across this cut.

There is a considerable difference in the cut efficiencies before the 'lepton' cut. In all of the events where no isolated leptons are reconstructed, the leptonic W boson is reconstructed

---

[5]track multiplicity is taken as the number of reconstructed charged particles.

[6]τ_{discr} defined by $\tau_{discr} = \left(\frac{2E_{lep}}{\sqrt{s}}\right)^2 + \left(\frac{m_W^{lep}}{m_W^{true}}\right)^2$

[7]$\Delta\Omega_{iso}$ defined as,

$$(\phi_{lep} - \phi_{had}) < \pi \rightarrow \Delta\Omega_{iso} = \sqrt{(\theta_{lep} - \theta_{had})^2 + (\phi_{lep} - \phi_{had})^2} \tag{4}$$

$$(\phi_{lep} - \phi_{had}) \geq \pi \rightarrow \Delta\Omega_{iso} = \sqrt{(\theta_{lep} - \theta_{had})^2 + (2\pi - |\phi_{lep} - \phi_{had}|)^2}. \tag{5}$$
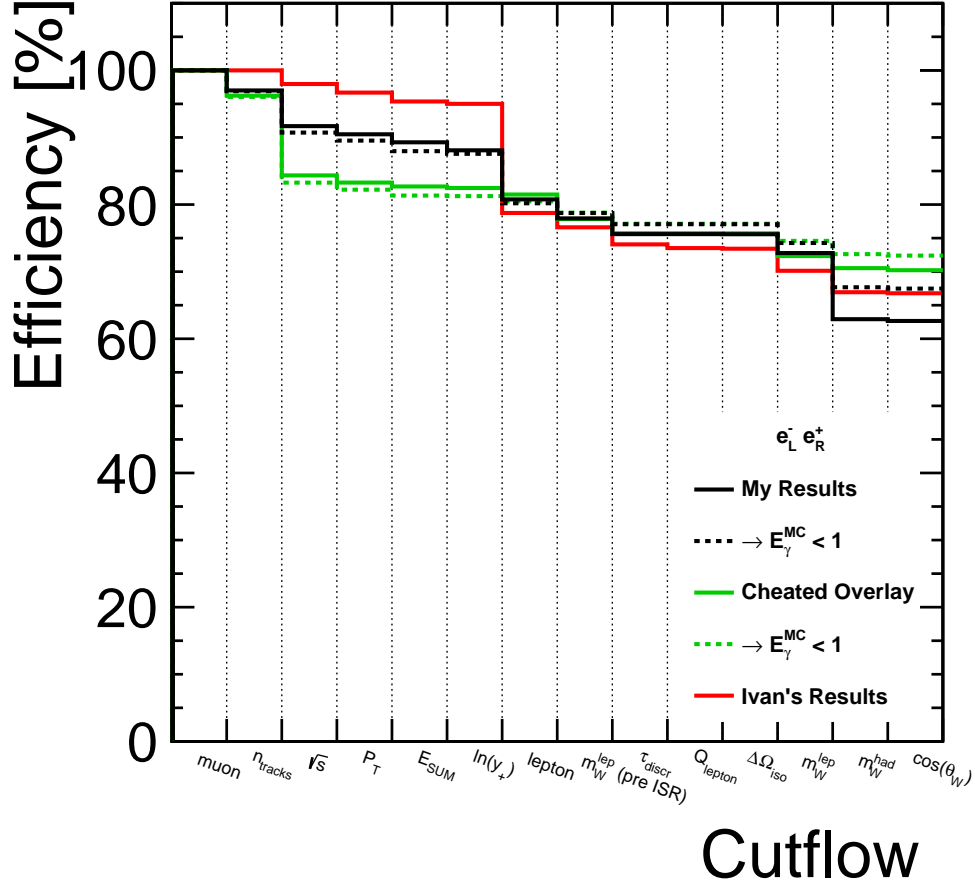
Figure 7: Cut flows comparing the results of this analysis (with and without cheating overlay removal) to previous studies. The results of this analysis considering a signal where $E_\gamma < 1$ are also displayed. The cuts on the x axis are as defined in Table. 1.

entirely from the invisible neutrino, will be completely wrong. The efficiency of the cheated and un-cheated background removal reconstructions converge on this lepton cut, suggesting that the differences observed before the cut are due to these incorrectly reconstructed events. When this lepton cut is applied to the current results before the rest of the cuts, the large discrepancy is not observed, providing support to this hypothesis (see Appendix. 7.2.5).

After the lepton cut, the efficiency of the reconstruction is higher than in previous studies, until the cut on the m_W^{had} where it is considerably worse. By looking at the cheated results though, which don't drop in efficiency as dramatically, it can be suggested that this is due to the performance of the beam background removal process. Further, after the lepton cut the $E_\gamma^{MC} < 1$ GeV signal is consistently performing better than the full signal, which suggests that large ISR energies reduces the efficiency of the reconstruction and so the detector.

3.2 Angle Cut Efficiencies

In this section the final result of the analysis, to evaluate the angular dependancy of the cut efficiency, is discussed. The efficiency is obtained for both the full signal and the $E_\gamma^{MC} < 1$ GeV signal, the results of which are shown in Figure. 8.
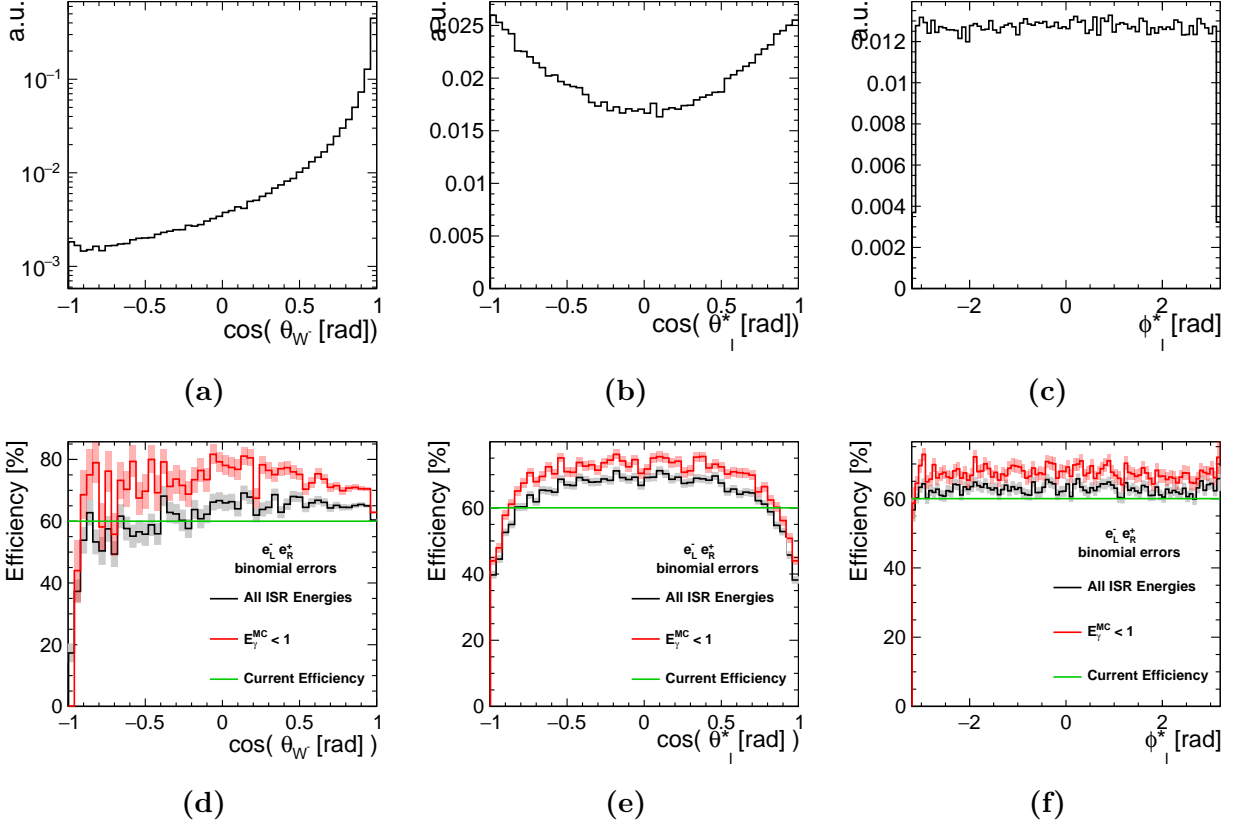
Figure 8: (a), (b) and (c) are the extracted angles as defined in Figure. 5.
(d), (e) and (f) are the associated cut efficiencies, after applying the cuts outlined in Table. 1.

The $\cos(\theta_{W^-})$ distribution is statistically limited towards -1, in the backwards direction, greatly reducing the efficiency. Due to the low mass of the neutrino, it becomes more virtual as more momentum is transferred to it, reducing the cross section. As a result most of the momentum transfer is to the W bosons, aligning it to the lepton it decayed from. In this case the W^- momentum is preferably aligned to the momentum of the e^- and so we see the angular distribution is highly biased towards the $\cos(\theta_{W^-}) = 1$ side. It is, however, reasonably constant throughout the rest of the distribution. The efficiency has a clear angular dependance on $\cos(\theta_l^*)$, with lower efficiency in regions closely aligned to the beam-pipe. Due to the coordinate system used this is not trivially explained, however for W bosons highly aligned to the beam pipe, the lepton appears to decay in a preferably transverse direction in the center of mass frame of such a boson. The ϕ_l^* of efficiency has a uniform efficiency as well as angular distribution, somewhat expected due to the uniformity of the W bosons ϕ distribution.

The $E_\gamma^{MC} < 1$ GeV signal has a higher efficiency than the full signal, but the angular dependance as a similar form. The magnitude of the efficiency differs by a constant factor.

4   Conclusion

The efficiency of the reconstruction of the semileptonic decay of a W pair produced in an $e_L^- e_R^+$ collision does have an angular dependence that is not currently modelled in the Electroweak Polarisation fit for the ILC. The theta coordinate of the negatively charged W boson, θ_{W^-}, is statistically limited in directions opposite to the initial electron's trajectory and so it is hard to observe the functional form of the efficiency dependance. The efficiency has a clear dependance on the theta coordinate of the lepton in the center of mass frame of the W it decayed from, θ_l^*.

There is a drop in efficiency as the leptons direction aligns with the beam pipe. There is no angular dependence observed in the efficiency as the phi coordinate of the lepton in the center of mass frame of the W it decayed from, ϕ_l^*, is varied.

It is also observed that the initial state radiation (ISR) does effect the efficiency of the reconstruction. For events with ISR energies below 1 GeV the reconstruction efficiency is higher by a constant factor, with a similar functional form. As the Electroweak Polarisation fit does not currently model ISR this is an important feature.

A significant drop in the efficiency of the reconstruction is due to the beam background removal and due to events where there is no reconstructed isolated lepton, otherwise this reconstruction is seen to perform similarly, and slightly better, than previous studies.

In future studies, the potential bias introduced by implementing the three ISR energy solutions in the reconstruction should be looked into and the appropriate cuts made. An alternative approach would be to perform a full kinematic fit to arrive at the best solution for the 4-momenta of the particles in the final state.

5 References

[1] Werner Herr and B Muratori. "Concept of luminosity". In: (2006). DOI: 10.5170/CERN-2006-002.361. URL: http://cds.cern.ch/record/941318.

[2] Matteo Cacciari, Gavin P. Salam, and Gregory Soyez. "FastJet User Manual". In: *Eur. Phys. J.* C72 (2012), p. 1896. DOI: 10.1140/epjc/s10052-012-1896-2. arXiv: 1111.6097 [hep-ph].

[3] Mikael Berggen. "Truth information : RecoMCTruthLinker and TrueJet". In: *Software & Analysis Pre-Meeting to ILD Workshop* (2018). URL: https://agenda.linearcollider.org/event/7839/contributions/40940/.

[4] Fons Rademakers et al. *root-project/root: First release of the v6-18 series.* July 2019. DOI: 10.5281/zenodo.3336325. URL: https://doi.org/10.5281/zenodo.3336325.

[5] C. Duerig and J. Tian. "isolated lepton finder". In: *GitHub repository* (2019). URL: https://agenda.linearcollider.org/event/6787/session/10/contribution/17/material/slides/0.pdf.

[6] J. Strube. "LCFIPlus". In: (2015). URL: https://confluence.slac.stanford.edu/display/ilc/LCFIPlus.

[7] M. Tanabashi et al. "Review of Particle Physics". In: *Phys. Rev. D* 98 (3 Aug. 2018), p. 030001. DOI: 10.1103/PhysRevD.98.030001. URL: https://link.aps.org/doi/10.1103/PhysRevD.98.030001.

[8] I. Marchesini. "Triple Gauge Couplings and Polarization at the *ILC and* Leakage in a Highly Granular Calorimeter". Hamburg University, Diss., 2011. Dr. Hamburg: Hamburg University, 2011. URL: https://bib-pubdb1.desy.de/record/94888.

[9] Robert Karl. "From the Machine-Detector Interface to Electroweak Precision Measurements at the ILC Beam-Gas Background, Beam Polarization and Triple Gauge Couplings". Bitte POF/Facility überprüfen, vielen Dank, Maren Stein; Dissertation, Universität Hamburg, 2019. Dissertation. Hamburg: Universität Hamburg, 2019, p. 330. DOI: 10.3204/PUBDB-2019-03013. URL: https://bib-pubdb1.desy.de/record/424633.

6   Acknowledgments

I would like to thank my supervisor Jakob Beyer for giving me a cool project and always providing instant support whenever I asked for help. Not only this but he provided help to the other summer students in the FLC group without complaint, which went really above and beyond. I'd also like to thank the rest of the FLC group for providing a welcoming environment for us, inviting us on group excursions in and outside of work. Further, Daniel Heuchel and Vladimir Borchanikovn were great office mates and were a pleasure to work alongside.

It was great getting to know the other summer students in the FLC group - Sukee Dharani, Andreas Loeshcke Centeno, Peter Mckeown and Lorenzo Cotrozzi. They are all wonderful people and made the long hours writing reports and presentations a lot more bearable, ordering pizza to the office was a terrific idea.

I'd like to thank all the summer students who organised group events on the weekends, like our excursions to Cuxhaven and Lübeck, and made any food for the community, the cultural food picnic on the last Sunday was fantastic. In particular Jana Wittmann, who organised many events and made many cakes, even delivering one at 5 am!

Finally I'd like to thank Olaf Behnke and the organisation team for all their hard work in making this summer programme run smoothly.

7 Appendix

7.1 Derivation of the ISR energy E_γ with non-trivial m_γ and m_ν

Our initial assumptions are that the system is in the center of mass frame with an invariant mass of 500 GeV. The system contains a visible 4-momentum $p^\mu = (E, p_x, p_y, p_z)$ and an invisible 4-momentum (a neutrino $p_\nu^\mu = (E_\nu, p_{\nu,x}, p_{\nu,y}, p_{\nu,z})$ and an ISR photon $p_\gamma^\mu = (E_\gamma, 0, 0, p_\gamma)$). Both the neutrino and the photon have a non trivial invariant mass leading to the following equations.

Conservation of 3-momentum

$$p_x + p_{\nu,x} = 0 \tag{6}$$
$$p_y + p_{\nu,y} = 0 \tag{7}$$
$$p_z + p_{\nu,z} + p_\gamma = 0 \tag{8}$$
$$\tag{9}$$

Conservation of Energy

$$E + E_\nu + E_\gamma = 500 \tag{10}$$

Energy-Momentum equations

$$E_\nu^2 = p_\nu^2 + m_\nu^2 \tag{11}$$
$$E_\gamma^2 = p_\gamma^2 + m_\gamma^2 \tag{12}$$
$$\tag{13}$$

For a unique solution of E_γ we require 2 more constraints on m_γ and m_ν which have yet to be imposed, but assuming these constraints are independent of E_γ we can arrive at a solution as follows.

From conservation of 3-momentum

$$p_\nu^2 = p_{\nu,x}^2 + p_{\nu,y}^2 + p_{\nu,z}^2 \tag{14}$$
$$= p_x^2 + p_y^2 + (p_\gamma + p_z)^2 \tag{15}$$
$$= p^2 + p_\gamma^2 + 2p_\gamma p_z \tag{16}$$
$$= p^2 + E_\gamma^2 - m_\gamma^2 + 2p_\gamma p_z \,. \tag{17}$$

Conservation of energy then gives us,

$$(500 - E)^2 - p^2 = (E_\nu + E_\gamma)^2 - p^2 \tag{18}$$
$$= E_\nu^2 + E_\gamma^2 - p^2 + 2E_\gamma E_\nu \tag{19}$$
$$= p_\nu^2 + m_\nu^2 + E_\gamma^2 - p^2 + 2E_\gamma E_\nu \,. \tag{20}$$

Substituting in the expression for p_ν,

$$(500 - E)^2 - p^2 = \cancel{p^2} + E_\gamma^2 - m_\gamma^2 + 2p_\gamma p_z + m_\nu^2 + E_\gamma^2 - \cancel{p^2} + 2E_\gamma E_\nu \tag{21}$$
$$(500 - E)^2 - p^2 + m_\gamma^2 - m_\nu^2 = 2(E_\gamma^2 + p_\gamma p_z + E_\gamma E_\nu) \tag{22}$$
$$= 2(\cancel{E_\gamma^2} + p_\gamma p_z + E_\gamma[500 - \cancel{E_\gamma} - E]) \tag{23}$$
$$= 2(p_\gamma p_z + 500E_\gamma - EE_\gamma) \,. \tag{24}$$

Where we have one again used conservation of energy.

For convenience lets define

$$\lambda = \frac{1}{2}[(500 - E)^2 - p^2 + m_\gamma^2 - m_\nu^2] \tag{25}$$

and use $E_\gamma^2 = p_\gamma^2 + m_\gamma^2$ to arrive at a solvable equation in E_γ .

$$\lambda = p_\gamma p_z + 500 E_\gamma - E E_\gamma \tag{26}$$

$$[\lambda - (500 - E) E_\gamma] = p_\gamma p_z \tag{27}$$

$$[\lambda - (500 - E) E_\gamma]^2 = (E_\gamma^2 - m_\gamma^2) p_z^2 \tag{28}$$

$$\lambda^2 - 2\lambda(500 - E) E_\gamma + (500 - E)^2 E_\gamma^2 = p_z^2 E_\gamma^2 - p_z^2 m_\gamma^2 \tag{29}$$

$$[(500 - E)^2 - p_z^2] E_\gamma^2 - 2\lambda(500 - E) E_\gamma + (\lambda^2 + p_z^2 m_\gamma^2) = 0 \tag{30}$$

This can be solved with the quadratic formula to give,

$$E_\gamma = \frac{\lambda(500 - E) \pm \sqrt{\lambda^2(500 - E)^2 - [(500 - E)^2 - p_z^2][\lambda^2 + p_z^2 m_\gamma^2]}}{(500 - E)^2 - p_z^2} \tag{31}$$

$$= \frac{\lambda(500 - E) \pm p_z \sqrt{\lambda^2 - [(500 - E)^2 - p_z^2] m_\gamma^2}}{(500 - E)^2 - p_z^2} . \tag{32}$$

As expected, the solution with $m_\gamma = m_\nu = 0$ reduces to the previously calculated solution

$$\lambda = \frac{1}{2}[(500 - E)^2 - p^2 + \cancel{m_\gamma^2}^{0} - \cancel{m_\nu^2}^{0}] \tag{33}$$

$$E_\gamma = \frac{\lambda(500 - E) \pm p_z \sqrt{\lambda^2 - [(500 - E)^2 - p_z^2]\cancel{m_\gamma^2}^{0}}}{(500 - E)^2 - p_z^2} \tag{34}$$

$$= \frac{\lambda[(500 - E) \pm p_z]}{(500 - E)^2 - p_z^2} \tag{35}$$

$$= \frac{\frac{1}{2}[(500 - E)^2 - p^2]}{(500 - E) \mp p_z} \tag{36}$$

$$= \frac{(500 - E)^2 - p^2}{1000 - 2E \mp 2p_z} . \tag{37}$$
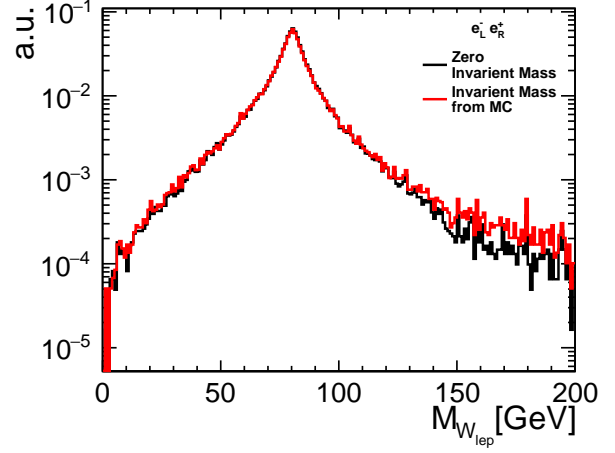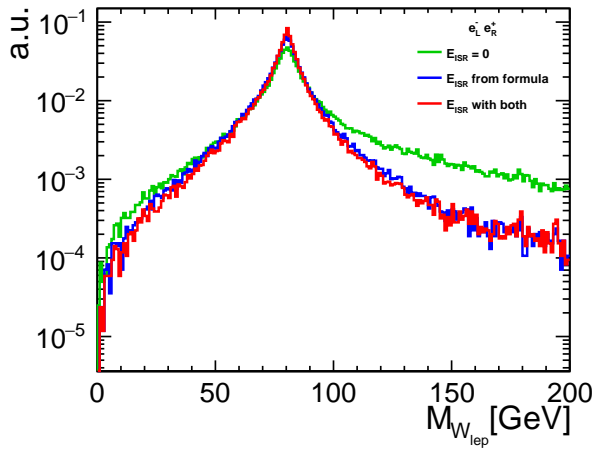
c.f Ivan's result [8]

It can also easily be shown for this case that the two solutions correspond to ISR photons travelling parallel or anti-parallel to the z axis. The $\mp$ in the denominator hence corresponds to the sign of the photons z momentum,

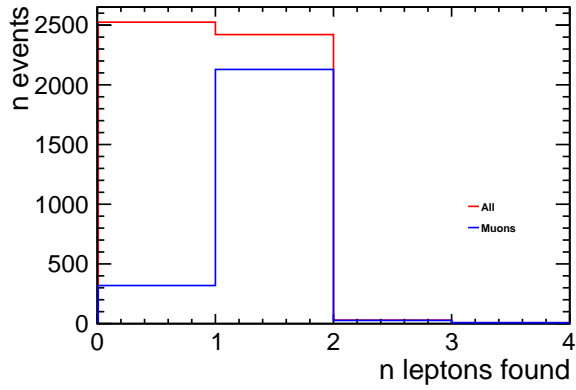$$E_\gamma = \frac{(500 - E)^2 - p^2}{1000 - 2E + 2sgn(p_\gamma)p_z} \tag{38}$$

$$E_\gamma = \frac{\lambda(500 - E) + sgn(p_\gamma)p_z \sqrt{\lambda^2 - [(500 - E)^2 - p_z^2]m_\gamma^2}}{(500 - E)^2 - p_z^2} . \tag{39}$$
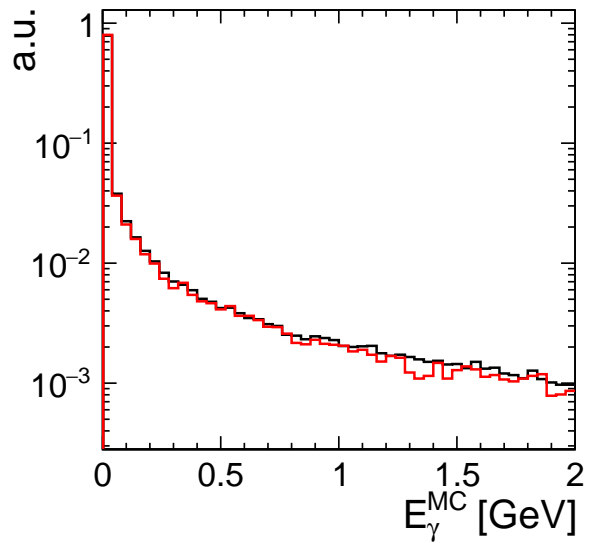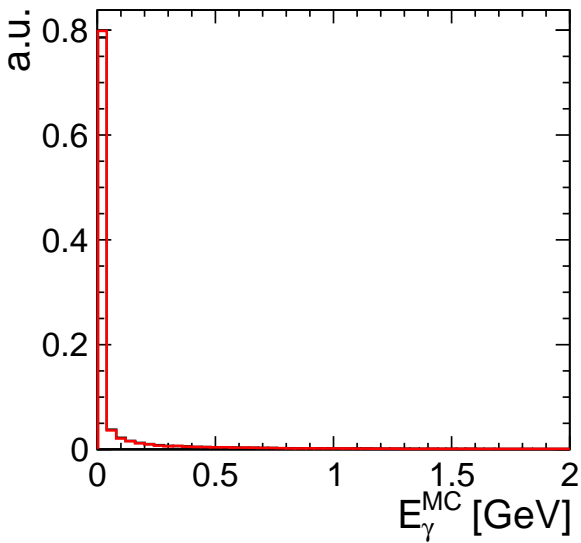
7.2 Backup Figures

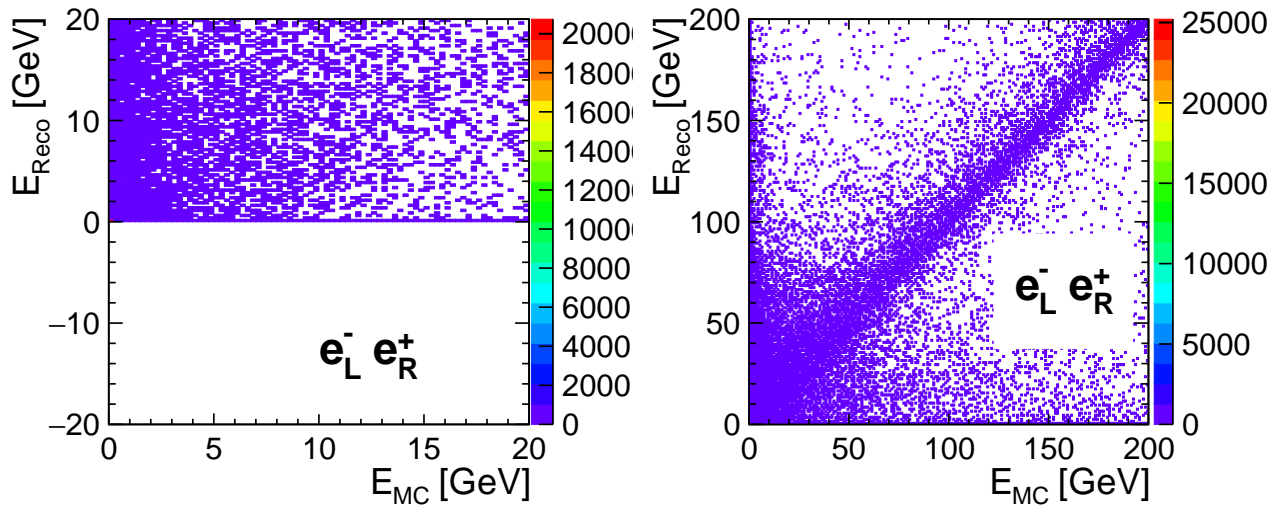### 7.2.1 Log plots of Mass reconstruction

7.2.2 Number of isolated leptons reconstructed

7.2.3 Generator level ISR mass

7.2.4 ISR energy reconstruction with all 3 solutions

7.2.5 Cut flow with lepton cut applied simultaneously with n_{tracks}